

High-accuracy scaling exponents in the local potential approximation

Claude Bervillier^a, Andreas Jüttner^b, and Daniel F. Litim^{c,d}

^a Laboratoire de Mathématiques et Physique Théorique, Université de Tours, Parc de Grandmont, F-37200 Tours

^b School of Physics and Astronomy, University of Southampton, Southampton SO17 1BJ, U.K.

^c Department of Physics and Astronomy, University of Sussex, Brighton, East Sussex, BN1 9QH, U.K.

^d Theory Group, Physics Division, CERN, CH-1211 Geneva 23.

We test equivalences between different realisations of Wilson's renormalisation group by computing the leading, subleading, and anti-symmetric corrections-to-scaling exponents, and the full fixed point potential for the Ising universality class to leading order in a derivative expansion. We discuss our methods with a special emphasis on accuracy and reliability. We establish numerical equivalence of Wilson-Polchinski flows and optimised renormalisation group flows with an unprecedented accuracy in the scaling exponents. Our results are contrasted with high-accuracy findings from Dyson's hierarchical model, where a tiny but systematic difference in all scaling exponents is established. Further applications for our numerical methods are briefly indicated.

I. INTRODUCTION

Renormalisation group (RG) methods provide powerful tools in the computation of universal scaling exponents or anomalous dimensions in quantum field theories [1]. Modern functional RG approaches are based on Wilson's idea to integrate-out momentum modes within a path-integral representation of the theory, *e.g.* [2]. A particular strength of these methods is their flexibility when it comes to approximations. Wilsonian flows can be implemented in many different ways, which helps adapting the technique to the problem at hand.

A useful systematic expansion scheme is the derivative expansion, which, to leading order, is known as the local potential approximation (LPA). For the study of critical phenomena, the derivative expansion is expected to provide good results as long as quantum corrections to propagators and anomalous dimensions remain small [3]. Important results in LPA have been accumulated over the years based on different implementations of the RG including the Wilson-Polchinski RG [4, 5], the functional RG [2] for the effective average action [6] and optimised versions thereof [7], and Dyson's hierarchical RG [8, 9]. Interestingly, and despite qualitative differences in the respective formalisms, these approaches are closely related in LPA. In fact, it has been established by Felder [10] that the Wilson-Polchinski RG and the hierarchical RG are equivalent. More recently, following a conjecture first stated in [11, 12], the equivalence between the Wilson-Polchinski flow and an optimised functional RG has been proven by Morris [13]. Consequently, universal scaling exponents from either of the three approaches should be identical.

Quantitatively, these equivalences have been put to test for 3d critical scalar theories [12, 14]. While

scaling exponents from either approach agree at the order 10^{-4} , an unexpected disagreement starting at the order 10^{-5} was found. Presently, however, this last observation solely relies on results from the hierarchical RG and the optimised RG, where exponents have been obtained with sufficiently high accuracy. Therefore it becomes mandatory to obtain results from the Wilson-Polchinski RG with a higher precision, in order to confirm or refute the above-mentioned discrepancy.

In this paper, we close this gap in the literature and study both the Wilson-Polchinski RG and the optimised RG for the 3d Ising universality class with an unprecedented accuracy. To that end, we introduce several methods to solve non-linear eigenvalue problems with special emphasis on the numerical reliability. We expect that these techniques are equally useful for other non-linear problems in mathematical physics. The outline of the paper is as follows. We introduce the relevant differential equations (Sec. II) and discuss our numerical methods (Sec. III) and the error control (Sec. IV). Results for the fixed point solution and scaling exponents are discussed (Sec. V) and compared with the hierarchical model (Sec. VI). We close with a discussion and conclusions (Sec. VII).

II. LOCAL POTENTIAL APPROXIMATION

We restrict ourselves to a real scalar field theory in three dimensions – the Ising universality class – and to the leading order in the derivative expansion, meaning that the scale-dependent effective action is approximated by $\Gamma_k = \int d^3x [\frac{1}{2}\partial_\mu\phi\partial_\mu\phi + V_k(\phi)]$. Here, k denotes the scale of the Wilsonian momentum cutoff. We provide the flows in terms of the dimensionless potentials $u(\rho) = V_k(\phi)/k^3$ with

$\rho = \frac{1}{2}\phi^2/k$, and $v(\varphi) = V_k(\phi)/k^3$ with $\varphi = \phi/\sqrt{k}$. Within an effective average action approach [6], the flow equation for $u(\rho)$ depends on the infrared momentum cutoff. For an optimised choice of the latter [7], and neglecting an irrelevant (field-independent) term, it is given by

$$\partial_t u = -3u + \rho u' + \frac{1}{1 + u' + 2\rho u''}. \quad (1)$$

Here, $t = \ln k$ denotes the logarithmic scale parameter. At a fixed point $\partial_t u' = 0$, the potential obeys

$$\frac{du''}{d\rho} = \left(\frac{u''}{2} - \frac{u'}{\rho} \right) (1 + u' + 2\rho u'')^2 - \frac{3u''}{2\rho}. \quad (2)$$

There exists a unique non-trivial and well-defined (finite, no poles) solution to (2) which extends over all fields. In terms of the potential $v(\varphi)$, the corresponding equations are

$$\partial_t v = -3v + \frac{1}{2}\varphi v' + \frac{1}{1 + v''}, \quad (3)$$

$$\frac{dv''}{d\varphi} = \frac{1}{2}(\varphi v'' - 5v')(1 + v'')^2. \quad (4)$$

For the Wilson-Polchinski RG, we follow an analogous ansatz for the effective action. In terms of the potential $u(\rho)$ and with $t = \ln k$ we find

$$\partial_t u = -3u + \rho u' - u' - 2\rho u'' + 2\rho(u')^2 \quad (5)$$

$$\frac{du''}{d\rho} = \frac{u''}{2} - \frac{u'}{\rho} + \frac{(u')^2}{\rho} + 2u' u'' - \frac{3u''}{2\rho}. \quad (6)$$

The corresponding equations for $v(\varphi)$ are

$$\partial_t v = -3v + \frac{1}{2}\varphi v' - v'' + (v')^2, \quad (7)$$

$$\frac{dv''}{d\varphi} = \frac{1}{2}(\varphi v'' - 5v') + 2v' v''. \quad (8)$$

Numerical solutions for the fixed point potentials and their derivatives (2), (4) and (8) are displayed in Figs. 1, 2, 3, 6 and 7 below.

The potential $v(\varphi)$ in (3) is related to the Wilson-Polchinski potential $v_{\text{WP}}(\varphi_{\text{WP}})$ in (7) by a Legendre transform [13],

$$v = v_{\text{WP}} + \frac{1}{2}(\varphi_{\text{WP}} - \varphi)^2, \quad (9)$$

$$\varphi = \varphi_{\text{WP}} - v'_{\text{WP}}, \quad (10)$$

up to an irrelevant constant (the absolute value of the potentials at vanishing field). An immediate consequence of (10) is that the two potentials take their absolute minimum at the same field value $\varphi_{\text{WP},0} = \varphi_0$. It follows that the barrier heights

$$v(0) - v(\varphi_0) = v_{\text{WP}}(0) - v_{\text{WP}}(\varphi_0) \quad (11)$$

are identical. Further similarities and differences between (1) – (8) have been studied in [12, 13].

III. NUMERICAL METHODS

In this section, we summarise the numerical techniques used to solve (1) – (8) and similar to high accuracy at a fixed point, and to deduce the leading and subleading scaling exponents. These include tools for local polynomial expansions with various degrees of sophistication (a) – (c), tools for initial-value problems (d), and tools for solving (two-point) boundary-value problems (e). Analytical methods for solving (1) can be found in [15, 16], and are not further elaborated here.

A. Local behaviour

For small fields, we use polynomial expansions of the effective potential [17]. Their convergence has been addressed in [15, 18, 19]. We implement the expansion in different ways (a) – (c). At a fixed point, the potential is Z_2 -symmetric under $\varphi \rightarrow -\varphi$. Therefore, we expand the effective potential in ρ rather than in φ .

(a) We Taylor-expand the potential $u(\rho)$ in field monomials about vanishing field $\sim \rho^n$ up to the maximum order m in the truncation,

$$u(\rho) = \sum_{n=1}^m \frac{1}{n!} \lambda_n \rho^n. \quad (12)$$

Inserting (12) into (1) and solving for $\partial_t u' = 0$ leads to coupled ordinary differential equations $\partial_t \lambda_n = \beta_n(\{\lambda_i\})$ for the couplings λ_i , which are solved numerically. We note that the m differential equations $\partial_t \lambda_n$ depend, in general, on $m+2$ couplings up to order λ_{m+2} . Therefore, we have to provide boundary conditions for the couplings λ_{m+1} and λ_{m+2} , as their values are undetermined by the truncated flow. For (12), we employ $\lambda_{m+1} = 0$ as a boundary condition (in an expansion about vanishing field, the dependence on λ_{m+2} drops out), which shows good convergence with increasing m ; see Tab. 1 for numerical results for the couplings at the fixed point of (1).

(b) The convergence is further enhanced by expanding $u(\rho)$ about non-vanishing field [15, 18]. In this case, we write

$$u(\rho) = \sum_{n=2}^m \frac{1}{n!} \lambda_n (\rho - \lambda_1)^n, \quad (13)$$

where the expansion point $\rho = \lambda_1$ is defined implicitly by $u'(\lambda_1) = c$ with c a free parameter. From (1) we conclude that c can take values between -1

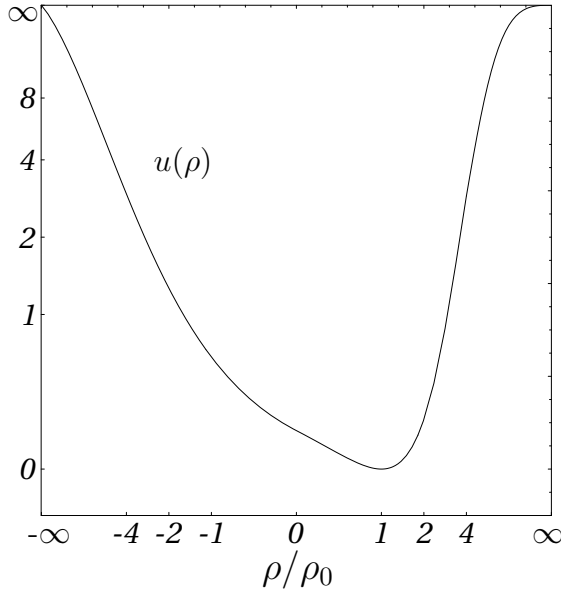


Figure 1: Fixed point potential $u(\rho)$ from (1), (2) of the Ising universality class for all fields $\rho \in [-\infty, \infty]$. The absolute minimum is at $\rho_0 = 1.814\ 898\ 403\ 687\cdots$, where the potential is normalised to $u(\rho_0) = 0$. The axes are rescaled as $x \rightarrow \frac{x}{2+|x|}$ with $x = \rho/\rho_0$, and $u \rightarrow \frac{u}{2+u}$.

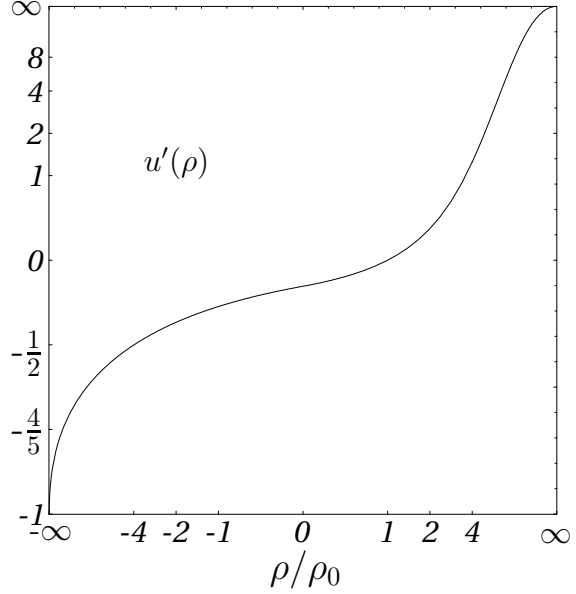


Figure 2: First derivative of the fixed point potential $u'(\rho)$ from (1), (2) in the Ising universality class. Numerically, it reads $u'(0) = -0.186\ 064\ 249\ 470\cdots$ at vanishing argument. u' is a monotonously increasing function of the field. Same rescaling as in Fig. 1 (see text).

and ∞ . This is confirmed by the explicit result, see Fig. 2. A natural choice is $c = 0$, in which case λ_1 denotes the unique potential minimum, $u'(\lambda_1) = 0$. The numerical convergence of the expansion is best for small c . In a given truncation to order m , the boundary condition $\lambda_{m+1} = 0 = \lambda_{m+2}$ is used. The expansion displays very good convergence properties with increasing m [15]; see Tab. 1 for numerical results for the couplings at the fixed point of (1).

(c) The simple boundary conditions $\lambda_{m+1} = 0$ or $\lambda_{m+1} = 0 = \lambda_{m+2}$ used in (a) or (b), respectively, fail to provide convergent solutions for the Wilson-Polchinski flow (5). The reason behind this is that the Wilson-Polchinski flow at small fields is more strongly sensitive to the couplings at large fields [12]. Identifying a stable solution is then more demanding and boils down to providing better-adapted boundary conditions for those higher order couplings, which are undetermined in a given truncation. Equations which fix the higher order couplings can be derived from the asymptotic behaviour of the scaling solution. An algebraic procedure which determines the highest order couplings from the asymptotic behaviour of (2), *i.e.* from $u'' \rightarrow 0$ for $\rho \rightarrow \infty$ [and similarly for (6)] has been given in [20]. We have adopted this

procedure for (6) (for technical details, see [21]). As a result, we find that the polynomial expansion (12) for the Wilson-Polchinski flow (6) with appropriate boundary condition converges nicely; see Tab. 2 for numerical results for the couplings at the fixed point of (5). Although it is more demanding to stabilise the small field expansion based on (5) as opposed to (1), we note that the Wilson-Polchinski potential for small fields differs only mildly from the optimised fixed point potential (see Fig. 6 below).

Polynomial expansions like (12) and (13) have, in general, a finite radius of convergence in field space, restricted to field values $\rho_{\min} \leq \rho \leq \rho_{\max}$. Here, we find that $\rho_{\min} < 0$ and $\rho_{\max} > \rho_0$.

In either of these cases (a) – (c), the flows (1) and (5) transform into a set of m coupled ordinary differential equations $\partial_t \lambda_n = \beta_n(\{\lambda_i\})$ for the coefficient functions λ_n . The fixed point equations $\beta_n(\{\lambda_i\}) = 0$ can be solved to very high accuracy with standard methods. The scaling exponent ν and subleading corrections-to-scaling exponents are deduced from the eigenvalues of the stability matrix M at criticality, $M_{ij} = \partial_{\lambda_i} \beta_j|_{\partial_t u' = 0}$. Asymmetric corrections-to-scaling, *i.e.* eigenperturbations not symmetric under $\varphi \rightarrow -\varphi$, can be obtained as well [22].

coupling	$\rho = 0$	$u'(\rho = \lambda_1) = 0$
λ_1	-0.186 064 249 470	1.814 898 403 687
λ_2	0.082 177 310 824	0.126 164 421 218
λ_3	0.018 980 341 099	0.029 814 964 767
λ_4	0.005 252 082 509	0.006 262 816 384
λ_5	0.001 103 954 106	-0.000 275 905 516

Table 1: The first five couplings at the fixed point of the optimised flow (1) at vanishing field (first column), and at the potential minimum (second column).

coupling	$\rho = 0$	$u'(\rho = \lambda_1) = 0$
λ_1^{WP}	-0.228 598 202 437	1.814 898 403 687
λ_2^{WP}	0.187 236 893 730	0.086 535 420 434
λ_3^{WP}	-0.105 930 606 484	-0.028 253 169 622
λ_4^{WP}	0.101 611 201 027	0.015 928 269 983
λ_5^{WP}	-0.135 786 295 049	-0.012 666 298 430

Table 2: The first five couplings at the fixed point of the Wilson-Polchinski flow (5) at vanishing field (first column), and at the potential minimum (second column).

B. Global behaviour

Next we discuss two methods (d) and (e) which integrate (2) or (6) directly, without using polynomial approximations.

(d) Initial value problem. The differential equations (2) or (6) are studied as initial value problems with boundary conditions given at some starting point ρ_1 . The necessary boundary conditions can be obtained within the polynomial expansion (a) and (b) in their domain of validity, see Tab. 1 for the couplings at vanishing field and at the potential minimum. The boundary conditions are

$$\begin{aligned} u'(0) &= \lambda_1, & u''(0) &\equiv \lambda_2 = -\frac{2}{3}\lambda_1(1 + \lambda_1)^2 \\ u'(0) &= \lambda_1^{\text{WP}}, & u''(0) &\equiv \lambda_2^{\text{WP}} = -\frac{2}{3}\lambda_1^{\text{WP}}(1 + \lambda_1^{\text{WP}}) \end{aligned}$$

at $\rho_1 = 0$ for the optimised RG flow [15] and the Wilson-Polchinski flow, respectively. Identifying the well-defined fixed point solution $u'(\rho)$ which extends over all fields ρ requires a high degree of fine-tuning in the boundary condition λ_1 [19]. Integrating (2) towards larger fields, starting at some non-vanishing field $|\rho| \sim \mathcal{O}(1)$ with boundary conditions from (a) or (b) is numerically more stable. Following this strategy, we have computed in Figs. 1, 2 and 3 the fixed point potential u , its first derivative u' , and the field-dependent mass term $u' + 2\rho u''$, respectively, for all $\rho \in [-\infty, \infty]$.

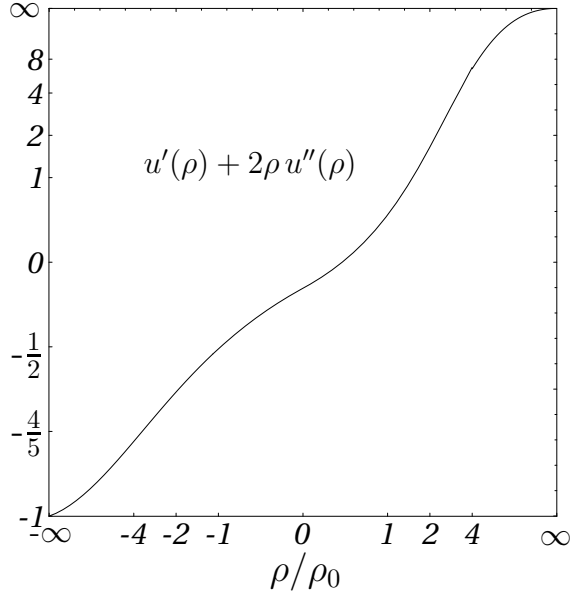


Figure 3: Mass function $u' + 2\rho u''$ of the fixed point potential (2) in three dimensions, Ising universality class. Same rescaling as in Fig. 1 (see text). For $\rho = \frac{1}{2}\varphi^2 \geq 0$, the mass function is equivalent to $v''(\varphi)$ from (4).

We note that u displays only one global minimum. Both u' and $u' + 2\rho u''$ are monotonously increasing functions of the field variable. The numerical solution fits the expected analytical behaviour for asymptotically large fields.

(e) Finally, we discuss solvers for two-point boundary value problems. The shooting method [23] requires boundary conditions at two points ρ_1 and ρ_2 in field space. Initial conditions at ρ_1 are varied until the boundary condition at ρ_2 is matched. The procedure is iterated until the desired accuracy in the solution is achieved [23]. If one is not constrained by the Z_2 symmetry $\varphi \rightarrow -\varphi$ and because of the potentially singular behaviour of the right-hand sides of (2) and (6) for $\rho \rightarrow 0$, it is preferable to implement (4) and (8). Then the differential equations at the origin $\varphi = 0$ are better under control and one may shoot from the origin $\varphi_1 = 0$ (with the required symmetry conditions imposed) to large fields $\varphi_2 \approx \varphi_{\text{bound}}$, where the asymptotic large-field behaviour is imposed. Shooting in the reverse direction may provide a better accuracy. The large-field behaviour of (2), (6) and (4), (8) has previously been determined in the literature, *e.g.* [12]. The RG eigenvalues are deduced from (1) or (5) in the vicinity of the fixed point solution. The implementation of (3), (4) and (7), (8) in terms of φ allows a direct computation of asymmetric correction-to-scaling exponents.

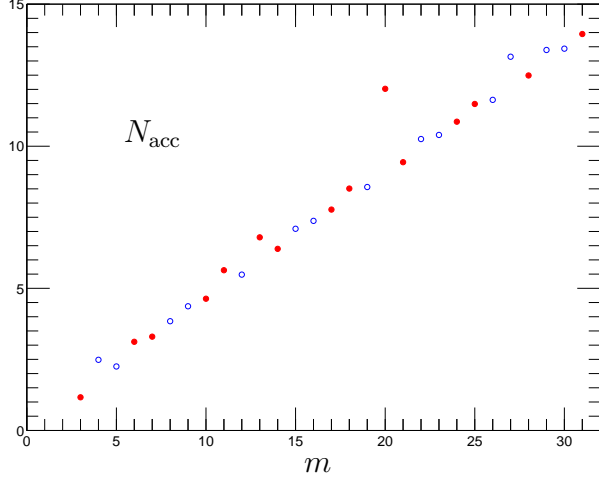


Figure 4: Accuracy of the fixed point, as defined in (14), and its dependence on the order of the expansion m ; from (1) using method (b) with $c = 0$.

IV. ERROR CONTROL

Within the numerical approaches (a) – (e), there are several sources for numerical errors, the control of which is discussed in this section.

(i) Within the polynomial expansions (a) – (c), the fixed point is determined by seeking simultaneous zeros of all β -functions. Solutions for $\partial_t \lambda_n = 0$ are found to very high precision. To ensure that the fixed point is numerically a good approximation to the full fixed point solution, we have computed $|\partial_t u'(\rho)|$ for all ρ within the domain of validity of the polynomial approximation. This serves as a measure for the quality of a polynomial expansion to order m . We define the accuracy N_{acc} of the fixed point solution to order m as

$$10^{-N_{\text{acc}}} = \max_{\rho \in [0, \rho_{\max}]} |\partial_t u'(\rho)|. \quad (14)$$

Here, $[0, \rho_{\max}]$ denotes a compact neighbourhood of the expansion point λ_1 , which needs not to coincide with the potential minimum ρ_0 . We take $\rho_{\max} > \rho_0$ from $u'(\rho_{\max}) + 2\rho_{\max} u''(\rho_{\max}) = 1$. This notion of accuracy is a good measure for how well a local Taylor expansion to order m approximates the full fixed point potential on $[0, \rho_{\max}]$. Using (b) with $c = 0$, we find that (14) achieves its extremum typically at $\rho = 0$. In Fig. 4, we display N_{acc} as a function of m . Full red (open blue) dots indicate that $\max \partial_t u'$ is positive (negative). The slope is approximately $1/2$, indicating that an increase in the truncation by $\Delta m \approx 2$ increases the accuracy

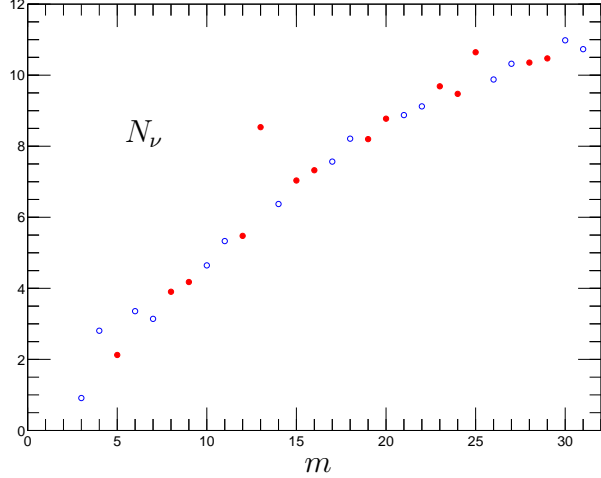


Figure 5: Accuracy of the scaling exponent ν , as defined by (15), and its dependence on the order of the expansion m ; from (1) using method (b) with $c = 0$.

in the fixed point solution roughly by a decimal place. This serves as an indicator for the reliability in the scaling exponents [see (ii)].

(ii) Within the polynomial expansions (a) – (c), we study the numerical convergence of both the fixed point values and the scaling exponents with increasing degree of truncation m [15]. In analogy to (14), we define the number of significant figures N_X in a fixed point coupling or a critical index X_m at order m in the expansion as

$$10^{-N_X} = \left| 1 - \frac{X_m}{X} \right|, \quad (15)$$

where X denotes the full (asymptotic) result. For the leading scaling exponent $X = \nu$, we display N_ν as a function of m in Fig. 5, based on the expansion (13) with $c = 0$. An open blue (full red) dot indicates that $\nu(m)$ is smaller (larger) than the asymptotic value. The expansion converges roughly in the pattern $++--$. Note that the slope, in comparison with Fig. 4, slightly decreases towards larger m . This part of the analysis is conveniently performed with MATHEMATICA. The accuracy of the matrix inversion (leading to the scaling exponents) has been checked independently with standard routines from MATLAB.

(iii) Within the polynomial expansions (a) and (b), we study the numerical stability of the result by varying the expansion point. The radius of convergence of polynomial expansions depends on the latter. This check serves as an indicator for a

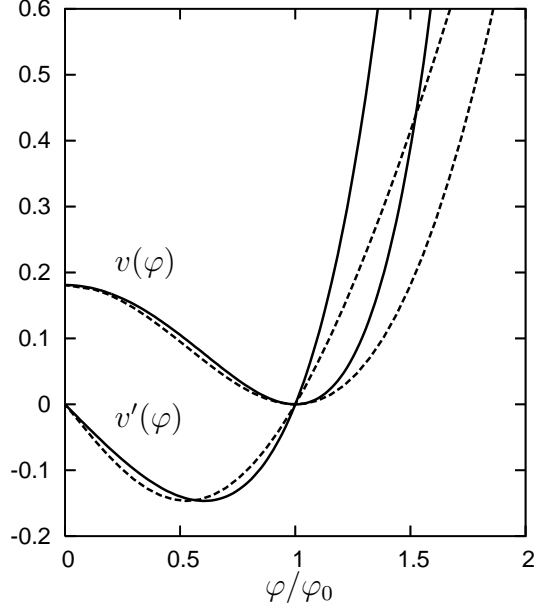


Figure 6: Comparison of the fixed point potentials $v(\varphi)$ and their first derivatives $v'(\varphi)$ from the optimised RG (full lines) and the Wilson-Polchinski RG (dashed lines). Both potentials are normalised to $v(\varphi_0) = 0$, where they take their absolute minimum. In either case, $\varphi_0 = \sqrt{2\rho_0} = 1.905\,202\,563\,344\cdots$.

possible break-down of the expansion at the highest orders. We have confirmed that only the rate of convergence depends on the expansion point, but not the asymptotic result.

(iv) The numerical approach (d) is checked in several ways. First, starting at intermediate fields, the numerical accuracy in the integration can be made large. Second, the domain of validity for (d) and (a) – (c) overlap. This allows for a quantitative cross-check. Third, for large fields $|\rho| \rightarrow \infty$, the results from (d) match the expected asymptotic behaviour. Fourth, we have cross-checked the result with a two-point boundary value routine.

(v) The shooting method (e) is controlled in several ways. First, the numerical precision for the solution on $[0, \rho_{\text{bound}}]$ is only limited by the machine precision. We use standard routines under **Fortran f77** with double precision. The boundary condition at large fields has not to be known to very high accuracy to achieve a reliable result. Stability in the result is confirmed by varying ρ_{bound} as well as the boundary condition at ρ_{bound} . These procedures are applied for both (2) and (6). The shooting method is checked independently using a different solver under **MAPLE**, based on a different boundary value integration algorithm.

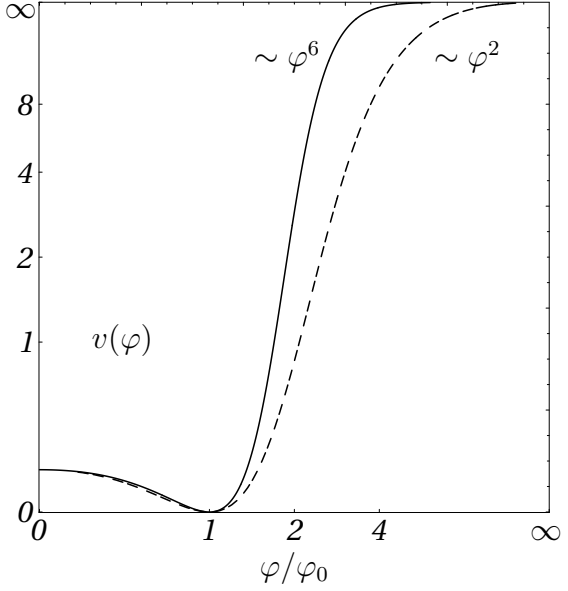


Figure 7: Comparison of the fixed point potentials $v(\varphi)$ from the optimised RG (full line) and the Wilson-Polchinski RG (dashed line) for all fields $\varphi \in [0, \infty]$. As in Fig. 6, the potentials are normalised to $v(\varphi_0) = 0$. For display purposes, the axes are rescaled as $x \rightarrow \frac{x}{2+|x|}$ with $x = \varphi/\varphi_0$, and $v \rightarrow \frac{v}{2+v}$.

V. RESULTS

Our results for the scaling exponents from (1) and (7) are given in Tab. 3 and 4. All digits are significant, except for possible rounding effects. Earlier findings with a lower level of accuracy [15, 24, 25] are fully consistent with Tab. 3. Specifically, in Tab. 3, the exponents from the optimised RG flows have been obtained using (a), (b), and (e), whereas those for the Wilson-Polchinski flow follow from (c) and (e). The method (b) has been used up to the order $m = 32$, leading to roughly 11 significant digits in the result for ν , and roughly one significant digit less with increasing order for the subleading exponents, see [15, 22]. Method (e) has been pushed to an accuracy of 14 digits for all scaling exponents. The asymmetric corrections-to-scaling exponents in Tab. 4 have been computed using (e), again to an accuracy of 14 digits. Again, all earlier results to lower order in the accuracy [22, 25] are consistent with Tab. 4.

In Figs. 1 – 3, we have plotted our results for the fixed point potential $u(\rho)$ from (2) and its derivatives for all $\rho \in [-\infty, \infty]$. It is noteworthy that the solution extends to all negative ρ , which in terms of the field φ corresponds to the analytical

exponent	optimised RG	Wilson–Polchinski RG
ν	0.649 561 773 880 65	0.649 561 773 880 65
ω	0.655 745 939 193 3	0.655 745 939 193 35
ω_2	3.180 006 512 059 2	3.180 006 512 059 2
ω_3	5.912 230 612 747 7	5.912 230 612 747 7
ω_4	8.796 092 825 414	8.796 092 825 414
ω_5	11.798 087 658 337	11.798 087 658 336 9
ω_6	14.896 053 175 688	14.896 053 175 688

Table 3: The leading scaling exponent ν and the first six subleading eigenvalues for the Ising universality class in three dimensions.

continuation to purely imaginary field values. For $\rho \rightarrow -\infty$, the solution approaches the convexity bound where $u' + 2\rho u'' \rightarrow -1$. In the flow equation (1), this limit is potentially singular as it corresponds to a pole. However, the explicit solution for $\partial_t u' = 0$ shows that the pole is suppressed, leading to a well-behaved solution even in this limit. In the physical domain where $\rho \geq 0$, the fixed point solution stays far away from the pole, since $\min_{\rho \geq 0}(u' + 2\rho u'') = u'(0) > -1$. General (non-fixed point) solutions to (1) approach the pole only in a phase with spontaneous symmetry breaking where $V''_k(\phi)$ is negative. Then the pole ensures convexity of the physical potential $V_{k=0}(\phi)$ in the infrared limit where $V''_{k=0}(\phi) \geq 0$ [26].

In Figs. 6 and 7, we compare the fixed point potentials $v(\varphi)$ from the optimised RG and the Wilson–Polchinski RG for small and large fields. We have checked that $u(\rho)$ in Fig. 1 matches $v(\varphi)$ in Fig. 7, as it should. Both potentials have their absolute minimum at the same field value $\rho_0^{\text{WP}} = \rho_0 = 1.814 898 403 687$; see Tab. 1 and 2. It is also confirmed that the potentials display the same barrier height $v(0) - v(\varphi_0)$ as expected from (11). For large fields, the potentials scale differently with the fields [12].

We have checked numerically that the fixed point solutions to (2) and (6) are related by a Legendre transform, see (9), (10). Consequently, at vanishing field, the couplings from Tab. 1 are related to the Wilson–Polchinski couplings in Tab. 2 by

$$\lambda_1 = \frac{\lambda_1^{\text{WP}}}{1 - \lambda_1^{\text{WP}}}, \quad \lambda_2 = \frac{\lambda_2^{\text{WP}}}{(1 - \lambda_1^{\text{WP}})^4}, \quad (16)$$

$$\lambda_1^{\text{WP}} = \frac{\lambda_1}{1 + \lambda_1}, \quad \lambda_2^{\text{WP}} = \frac{\lambda_2}{(1 + \lambda_1)^4}. \quad (17)$$

Similar expressions are found for the higher order couplings. The numerical results in Tab. 1 and 2 confirm these relations within the present accuracy.

exponent	optimised RG	Wilson–Polchinski
$\bar{\omega}$	1.886 703 838 091 4	1.886 703 838 091 4
$\bar{\omega}_2$	4.524 390 733 670 8	4.524 390 733 670 8
$\bar{\omega}_3$	7.337 650 643 354	7.337 650 643 354 4
$\bar{\omega}_4$	10.283 900 724 026	10.283 900 724 026

Table 4: The first four asymmetric correction-to-scaling exponents for the Ising universality class in three dimensions.

Our value $\lambda_1^{\text{WP}} = -0.228 598 202 437 02$ for the dimensionless mass term squared at vanishing field deviates at the order 10^{-5} from the corresponding value $-0.228 601 293 102$ given in [27].

In summary, we have confirmed the equivalence of an optimised RG and the Wilson–Polchinski RG to the order 10^{-14} in the universal indices, and in the Legendre-transformed fixed point solutions.

VI. COMPARISON

Next we compare our results with those based on Dyson’s hierarchical renormalisation group [8]. To leading order in the derivative expansion it has been proven by Felder [10] that the hierarchical RG is equivalent to the Wilson–Polchinski RG, and hence to the optimised RG. In particular, scaling exponents should come out identical. With high-accuracy numerical data at hand, we can test this assertion quantitatively.

In Tab. 5, we compare our results with previous computations of ν from the Wilson–Polchinski RG [27, 28], the optimised RG [11, 15], and the hierarchical RG [14, 29–34]. The most advanced hierarchical RG (HRG) and functional RG (FRG) studies agree amongst themselves at least to the order 10^{-6} and 10^{-12} , respectively. We emphasize that the functional RG results clearly deviate from the hierarchical RG results, although the difference $(\nu_{\text{FRG}} - \nu_{\text{HRG}})/\nu_{\text{FRG}} \approx -1.3 \times 10^{-5}$ is quantitatively small.

In Tab. 6 we compare the best results from the functional RG (*i.e.* from both the Wilson–Polchinski RG and the optimised RG) with those from the hierarchical RG for various other indices, some of which have been obtained with up to 12 significant figures [31] (see also [14]). The variations $(X_{\text{FRG}} - X_{\text{HRG}})/X_{\text{FRG}}$ in the exponents $X = \nu, \omega, \gamma, \Delta, \alpha$ read $(-1.3, 1.5, -1.3, 0.15, 5.0) \times 10^{-5}$, respectively. Hence, we confirm that the findings disagree, beginning at the order 10^{-5} .

Wilson – Polchinski	optimised RG	hierarchical RG
0.649 ^c	0.64956 ^g	0.6496 ^a
0.6496 ^d	0.649562 ^h	0.64957 ^b
0.649561773881	0.649561773881	0.649570 ^{e,f,i}

Table 5: Comparison of the scaling exponent ν for the Ising universality class in three dimensions (see text). Data from this work, and from *a)* [29], *b)* [30], *c)* [27], *d)* [28], *e)* [31], *f)* [32], *g)* [11], *h)* [15], *i)* [14].

exponent	functional RG	hierarchical RG
ν	0.649 561 773 880 65	0.649 570 ^{e,f,i}
ω	0.655 745 939 193 3	0.655 736 ⁱ
γ	1.299 123 547 761 3	1.299 140 730 159 ^e
Δ	0.425 947 495 477 4	0.425 946 859 881 ^e
α	0.051 314 678 358 05	0.051 289 ⁱ

Table 6: Comparison of universal indices ν , ω , $\gamma = 2\nu$, $\Delta = \omega\nu$ and $\alpha = 2 - 3\nu$ (for $\eta = 0$) from the functional RG (this work) and the hierarchical RG (same referencing as in Tab. 5).

VII. DISCUSSION AND CONCLUSIONS

Equivalences between non-linear differential or difference equations, and more generally functional relationships between different implementations of the renormalisation group, often allow for a deeper understanding of both the underlying physics and the adequacy and efficiency of the methods at hand. It has been proven previously that three different implementations of Wilson’s renormalisation group – the Wilson-Polchinski RG, an optimised version of the effective average action RG, and Dyson’s hierarchical RG – are equivalent in the local potential approximation. This implies that the corresponding non-linear RG equations should carry the identical universal content, *e.g.* identical scaling exponents.

Quantitatively, these equivalences have been confirmed up to the order 10^{-4} in the literature, but a discrepancy at the order 10^{-5} has recently been pointed out. This last observation followed from studies within Dyson’s hierarchical RG and an optimised RG where results with a sufficiently high accuracy are available, while previous results from the Wilson-Polchinski RG were in agreement with either of them. Here, we have closed this gap in the

literature by computing scaling exponents for the Ising universality class from the Wilson-Polchinski RG and the optimised RG with an unprecedented accuracy of the order 10^{-14} . We confirm their equivalence, first conjectured in [11], based on the leading, subleading and asymmetric correction-to-scaling exponents. Equally important, our central numerical results are obtained in several ways, and furthermore independently from both the Wilson-Polchinski and the optimised RG flow. We conclude that their equivalence is rock solid for all technical purposes, and in full agreement with the explicit proof given by Morris [13].

In contrast to this, we now have clear indications for a non-equivalence of our results with those from Dyson’s hierarchical model. In the $3d$ Ising universality class, all scaling exponents from the functional RG, *i.e.* from both the Wilson-Polchinski and the optimised RG, differ systematically at the order 10^{-5} from high accuracy studies based on Dyson’s hierarchical RG. This observation is in direct conflict with the proof of equivalence provided by Felder [10]. Given the high degree of accuracy in the critical indices from the present and earlier studies, and the fact that the scaling exponents in all three approaches have been obtained from several independent numerical implementations and collaborations, it would seem unlikely that the discrepancy originates from numerical insufficiencies. Presently, however, we cannot offer an explanation for this deviation. A deeper understanding of the quantitative mismatch between the functional RG and the hierarchical RG at the present order is desirable, also in view of extended truncations beyond the local potential approximation.

For our numerical work, we have developed methods to solve non-linear eigenvalue problems with high precision. The combined use of local polynomial expansions techniques with global integration methods allows for an efficient determination of the full fixed point solutions with reasonable numerical efforts. We have also put some emphasis on a reliable error control, in view of the high accuracy aimed for in the universal eigenvalues. We expect that this combination of techniques will be equally useful for other non-linear problems in mathematical physics, including *e.g.* the derivative expansion to higher order.

Acknowledgements. We thank Humboldt University for computer time. AJ is supported by PPARC grants PPA/G/S/2002/00467 and PPA/G/O/2002/0046. DFL is supported by an EP-SRC Advanced Fellowship.

[1] J. Zinn-Justin, *Quantum Field Theory And Critical Phenomena*, Oxford, Clarendon (1989); A. Pelissetto and E. Vicari, Phys. Rept. **368** (2002) 549 [cond-mat/0012164].

[2] C. Bagnuls and C. Bervillier, Phys. Rept. **348** (2001) 91 [hep-th/0002034]; J. Berges, N. Tetradis and C. Wetterich, Phys. Rept. **363** (2002) 223 [hep-ph/0005122]; J. Polonyi, Central Eur. J. Phys. **1** (2003) 1 [hep-th/0110026].

[3] G. R. Golner, Phys. Rev. **B33** (1986) 7863; D. F. Litim, JHEP **0111** (2001) 059 [hep-th/0111159].

[4] K. G. Wilson and J. B. Kogut, Phys. Rept. **12** (1974) 75.

[5] J. Polchinski, Nucl. Phys. B **231** (1984) 269.

[6] C. Wetterich, Phys. Lett. B **301** (1993) 90.

[7] D. F. Litim, Phys. Rev. D **64** (2001) 105007 [hep-th/0103195]; Phys. Lett. B **486** (2000) 92 [hep-th/0005245].

[8] F. J. Dyson, Commun. Math. Phys. **12** (1969) 91.

[9] G. Baker, Phys. Rev. B **5** (1972) 2622.

[10] G. Felder Commun. Math. Phys. **111** (1987) 101.

[11] D. F. Litim, Int. J. Mod. Phys. A **16** (2001) 2081 [hep-th/0104221].

[12] D. F. Litim, JHEP **0507** (2005) 005 [hep-th/0503096].

[13] T. R. Morris, JHEP **0507** (2005) 027 [hep-th/0503161].

[14] J. J. Godina, L. Li, Y. Meurice and M. B. Oktay, Phys. Rev. D **73** (2006) 047701 [hep-th/0511194].

[15] D. F. Litim, Nucl. Phys. B **631** (2002) 128 [hep-th/0203006].

[16] N. Tetradis and D. F. Litim, Nucl. Phys. B **464** (1996) 492 [hep-th/9512073], D. F. Litim and N. Tetradis, hep-th/9501042.

[17] A. Margaritis, G. Odor and A. Patkos, Z. Phys. C **39** (1988) 109; N. Tetradis and C. Wetterich, Nucl. Phys. B **422** (1994) 541 [hep-ph/9308214]; M. G. Alford, Phys. Lett. B **336** (1994) 237 [hep-ph/9403324].

[18] K. I. Aoki, K. i. Morikawa, W. Souma, J. i. Sumi and H. Terao, Prog. Theor. Phys. **95** (1996) 409 [hep-ph/9612458], Prog. Theor. Phys. **99**, 451 (1998) [hep-th/9803056].

[19] T. R. Morris, Phys. Lett. B **334** (1994) 355 [hep-th/9405190].

[20] B. Boisseau, P. Forgacs and H. Giacomini, hep-th/0611306.

[21] C. Bervillier, in preparation.

[22] D. F. Litim and L. Vergara, Phys. Lett. B **581** (2004) 263 [hep-th/0310101], M. M. Tsypin, Nucl. Phys. **B636**, 601 (2002) [hep-lat/0112001].

[23] W. H. Press, S. A. Teukolsky, W. T. Vetterling and B. P. Flannery, in *Numerical Recipes – The Art of Scientific Computing*, Cambridge University Press (1992).

[24] J. Comellas, Nucl. Phys. B **509** (1998) 662 [hep-th/9705129].

[25] C. Bervillier, Phys. Lett. A **332** (2004) 93 [hep-th/0405025].

[26] D. F. Litim, J. M. Pawłowski and L. Vergara, hep-th/0602140.

[27] R. D. Ball, P. E. Haagensen, J. I. Latorre and E. Moreno, Phys. Lett. B **347** (1995) 80 [hep-th/9411122].

[28] J. Comellas and A. Travesset, Nucl. Phys. B **498** (1997) 539 [hep-th/9701028].

[29] K. Wilson (private communication), in: [9], (5.41).

[30] K. Pinn, A. Pordt and C. Wieczorkowski, J. Statist. Phys. **77** (1994) 977 [hep-lat/9402020].

[31] J. J. Godina, Y. Meurice and M. B. Oktay, Phys. Rev. D **59** (1999) 096002 [hep-lat/9810034].

[32] J. Gottker-Schnetmann, cond-mat/9909418.

[33] J. J. Godina, Y. Meurice and M. B. Oktay, Phys. Rev. D **57** (1998) 6581 [hep-lat/9802001].

[34] J. J. Godina, Y. Meurice, M. B. Oktay and S. Niermann, Phys. Rev. D **57** (1998) 6326 [hep-lat/9709097].